AGU100 ADVANCING EARTH AND SPACE SCIENCE

Geophysical Research Letters

RESEARCH LETTER
10.1029/2018GL077868

Special Section:
Cassini's Final Year: Science Highlights and Discoveries

The Ion Composition of Saturn's Equatorial Ionosphere as Observed by Cassini

T. E. Cravens[1], L. Moore[2], J. H. Waite Jr.[3], R. Perryman[3], M. Perry[4], J.-E. Wahlund[5], A. Persoon[6], and W. S. Kurth[6]

[1]Department of Physics and Astronomy, University of Kansas, Lawrence, KS, USA, [2]Center for Space Physics, Boston University, Boston, MA, USA, [3]Space Science and Engineering Division, Southwest Research Institute, San Antonio, TX, USA, [4]Applied Physics Laboratory, Johns Hopkins University, Laurel, MD, USA, [5]Swedish Institute of Space Physics, Uppsala, Sweden, [6]Department of Physics and Astronomy, University of Iowa, Iowa City, IA, USA

Key Points:
- A heavy molecular species in Saturn's atmosphere is needed to explain the measured ion composition
- Measured ion and electron densities in the main Saturn ionosphere can be explained by solar ionizing radiation
- Both neutral and plasma measurements made at Saturn by Cassini suggest a strong ring-atmosphere interaction

Correspondence to:
T. E. Cravens,
cravens@ku.edu

Citation:
Cravens, T. E., Moore, L., Waite, J. H., Jr., Perryman, R., Perry, M., Wahlund, J.-E., et al. (2019). The ion composition of Saturn's equatorial ionosphere as observed by Cassini. *Geophysical Research Letters*, *46*, 6315–6321. https://doi.org/10.1029/2018GL077868

Received 13 MAR 2018
Accepted 11 MAY 2018
Accepted article online 21 MAY 2018
Published online 19 JUN 2019

Abstract The Cassini Orbiter made the first in situ measurements of the upper atmosphere and ionosphere of Saturn in 2017. The Ion and Neutral Mass Spectrometer (INMS) found molecular hydrogen and helium as well as minor species including water, methane, ammonia, and organics. INMS ion mode measurements of light ion species (H^+, H_2^+, H_3^+, and He^+) and Radio and Plasma Wave Science instrument measurements of electron densities are presented. A photochemical analysis of the INMS and Radio and Plasma Wave Science data indicates that the major ion species near the ionospheric peak must be heavy and molecular with a short chemical lifetime. A quantitative explanation of measured H^+ and H_3^+ densities requires that they chemically react with one or more heavy neutral molecular species that have mixing ratios of about 100 ppm.

Plain Language Summary Solar ultraviolet radiation is absorbed by Saturn's upper atmosphere and produces electrically charged molecules (or ions) and electrons in a region called the ionosphere. The Ion and Neutral Mass Spectrometer (INMS) instrument onboard the Cassini Orbiter made the first direct measurements of the composition of Saturn's ionosphere when the Cassini spacecraft flew through the upper atmosphere in the equatorial region. This paper reports on INMS measurements of the abundances of ionospheric protons, charged molecular hydrogen and helium, and protonated molecular hydrogen as functions of altitude and latitude. The paper also describes a photochemical analysis of the data indicating the presence in the upper atmosphere of heavy molecular species such as water, methane, and ammonia, thought to come from the rings. The deduced mixing ratio of these species relative to hydrogen is about a part in 10,000, which is consistent with measurements made using the neutral mode of the INMS. The simple chemical analysis was also able to reproduce the densities of electrons measured by the Radio and Plasma Wave Science instrument onboard Cassini. This paper contributes to our growing appreciation of the strong effect that the rings have on Saturn's atmosphere.

1. Introduction

Saturn's ionosphere was observed by the Pioneer 11 and the Voyager spacecraft (e.g., Kliore et al., 1980) using the radio occultation technique. The measured electron densities were much less than theoretical models of that time predicted (Waite et al., 1979). Electrostatic wave detection by the Voyager planetary radio astronomy investigation confirmed that peak electron densities were $\approx 10^4$ cm^{-3} or less (Kaiser et al., 1984) as did Cassini epoch radio occultation measurements made at the terminator (Kliore et al., 2009; Nagy et al., 2006).

The major neutral species in the atmosphere are molecular hydrogen and helium. Ionization of H_2 produces H_2^+ ions (≈90%) or H^+ ions (≈10%). H_2^+ ions rapidly react with H_2, producing H_3^+ ions, which can rapidly dissociatively recombine with electrons. However, electron recombination with H^+ ions is radiative, which is a very slow process. Among the suggestions made for reducing the predicted electron density was the reaction of H^+ with water coming from the rings, creating molecular ion species (H_2O^+ and then H_3O^+) with short chemical lifetimes (Connerney & Waite, 1984; Moore et al., 2010). Infrared observations of ionospheric H_3^+ have shown latitudinal structure that appears to be related to ring structure, suggesting that ions could also be traveling from the rings to the ionosphere along magnetic field lines (O'Donoghue et al., 2013).

The first in situ measurements of Saturn's upper atmosphere and ionosphere were made by the Cassini spacecraft in 2017 on the dayside (i.e., solar zenith angle about 20°), although information on the thermosphere from remote measurements was available earlier (e.g., Koskinen et al., 2015). The closed source neutral mode of the Ion and Neutral Mass Spectrometer (INMS) found that molecular hydrogen and helium were the major neutrals, but many minor species were also observed, including water, methane, carbon dioxide, ammonia, and organic compounds (Waite et al., 2018—herein called W18; Perry et al., 2018). The RPWS Langmuir probe measured the electron density (N_e) along the spacecraft track (Wahlund et al., 2017), and RPWS upper hybrid wave measurements gave independent determinations of N_e (Hadid et al., 2018; Persoon et al., 2019). Grains were detected in the upper atmosphere and exosphere extending to the D ring by the Magnetosphere Imaging Instrument Ion and Neutral Camera and Charge Energy Mass Spectrometer experiments (Mitchell et al., 2018). The present paper describes Cassini INMS composition measurements made with the open source ion mode. The paper also provides an empirical interpretation of the ion composition allowing heavy neutral species mixing ratios to be deduced. Related papers in this same special 2018 GRL issue include Hadid et al. (2018), Moore et al. (2018), Morooka et al. (2019), Perry et al. (2018), Persoon et al. (2019), and Yelle et al. (2018), particularly Moore et al. (2018).

2. INMS Instrument and Proximal Orbit Geometry

The INMS instrument is a radio-frequency quadrupole mass spectrometer that measures both ion and neutral composition in its open source ion and closed source neutral modes, respectively (Waite et al., 2004). The spacecraft (s/c) velocity with respect to Saturn during the proximal orbits was 31 km/s, which corresponds to 25 times higher kinetic energy per nucleon for incident molecules than during the Titan encounters. Heavier neutral species, or even grains, break up in the closed source antechamber at these speeds (Teolis et al., 2010). INMS ion measurements at these speeds limit observable ion species to those with mass numbers less than 8 Da (i.e., only lighter ions).

The derivation of densities, n_j, where j is mass number, from instrumental counts, C_j, per integration period, Δt = 0.031 s, has been described elsewhere (see Waite et al., 2004) but can be expressed as $C_j = (10^{-5}\ n_j)/(S_j\ u_{s/c}\ \Delta t)$, where S_j is a sensitivity factor that depends on mass number and $u_{s/c}$ = 32 km/s (for the Cassini proximal orbits) is the s/c speed in km/s. Values of S_j for Titan-like speeds were found during instrument calibration in the lab but Saturn conditions are different, leaving about a factor of 2 uncertainty. However, comparison of m = 1 (H^+) and m = 3 (H_3^+) densities measured by INMS and electron densities measured by RPWS (e.g., Persoon et al., 2019; Wahlund et al., 2017) strongly constrain S_1 and S_3 to much better than this factor (S_1 = 0.006 and S_3 = 0.0011). From very simple and known H_2^+ chemistry (discussed later), we find that S_2 = 0.0010. We arbitrarily adopt $S_4 = S_3$. Note that extensive laboratory calibration (cf. Waite et al., 2004) confirms the overall reasonableness of these values.

The s/c entered the atmosphere in the Northern Hemisphere and crossed the ring plane (equatorial plane) at a radial distance of r = 62,170 km for Cassini proximal orbit P288 (see W18). Closest approach (CA) was reached in the southern hemisphere at a distance below the equatorial plane of −7,421 km, or a latitude of $\lambda \approx -7$, or a planetocentric radial distance of r = 61,908 km, or a height above the 1-bar atmospheric level of ≈1,710 km (see Mueller-Wodarg et al., 2006, for information on atmospheric structure). The maximum neutral density was found at $\lambda \approx -4.5°$.

3. Overview of Ionospheric Data

Figure 1 shows INMS densities versus time from CA for ion mass numbers 1, 2, 3, and 4, with probable identifications of H^+, H_2^+, H_3^+, and He^+, respectively, although deuterated species D^+, HD^+, and H_2D^+ might make minor contributions to these mass signals.

The neutral density decreases with altitude exponentially as one would expect (see W18 for a presentation of INMS H_2 density data). The measured H_2 density at CA for P288 was 7×10^9 cm^{-3} and at the equatorial plane ($z = 0$ or latitude $\lambda = 0°$) was 1.5×10^8 cm^{-3}. The H^+ and electron densities are almost equal at higher altitudes, but H_3^+ is an important species at lower altitudes. At the lowest altitudes near CA, and spanning the equatorial region, the total ion density measured by INMS (i.e., light ions) falls well short of the measured electron density. This density "gap" points to the existence of heavier ion species with mass numbers exceeding

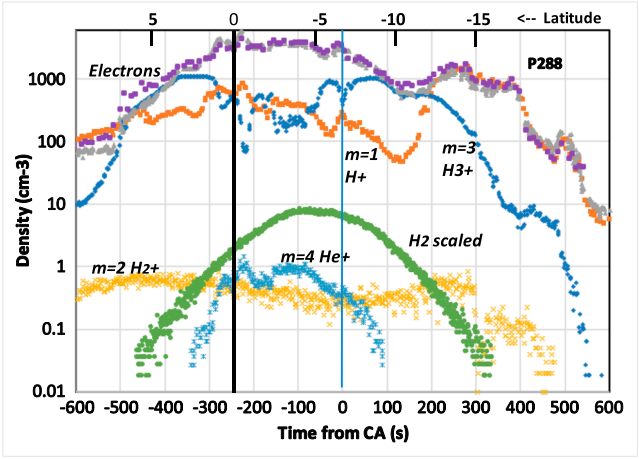

Figure 1. Ion and electron densities measured by the Cassini Ion and Neutral Mass Spectrometer open source ion and the Radio and Plasma Wave Science (RPWS) instruments are shown as a function of time from closest approach for P288. Latitude is also shown. Electron density measurements are from both the Langmuir probe (RPWS-LP; gray triangles) and from upper hybrid wave data (shown as filled purple squares). The heavy vertical line indicates the equatorial plane (latitude = 0°) crossing and the light vertical line indicates the time of closest approach (CA) of Cassini to Saturn. The neutral H_2 density measured by INMS (scaled down by a factor of 10^9) is also shown. The statistical errors are evident in the scatter of the points and are small except for H_2^+ and He^+.

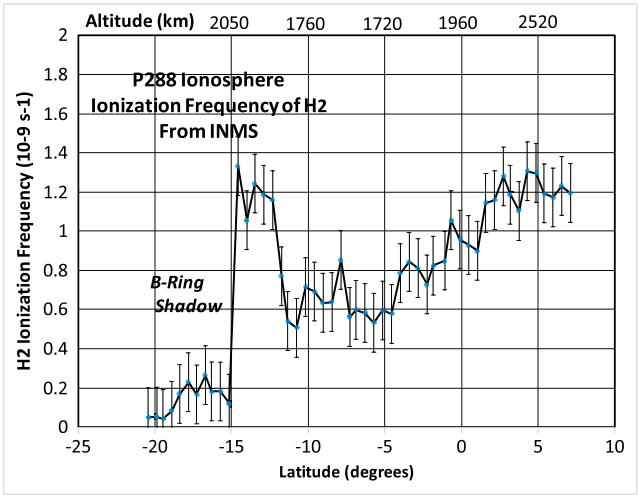

Figure 2. Photoionization frequency (i.e., production rate per neutral) of H_2 (which produces H_2^+ ions) for solar extreme ultraviolet radiation derived from Ion and Neutral Mass Spectrometer (INMS)-measured H_2 and H_2^+ densities for P288 versus latitude. An altitude scale is shown at top. Note that the maximum H_2 density is not quite at closest approach ($\lambda \approx -6.8°$) but is closer to the equator at $\lambda \approx -4.5°$. The statistical uncertainty associated with raw counts at closest approach is indicated and is applied to all points for simplicity. The B-ring shadow is indicated—also see Figure 1.

the INMS limit of 8 Da. The He^+ density profile ($m = 4$) follows from the measured neutral He density and the expected ion chemistry for this species (see Moore et al., 2018). The H_2^+ density is quite low ($n_{H2+} \approx 0.6$ cm^{-3}) and is associated with the major ionization process, as discussed in the next section.

4. Simple Ionospheric Chemistry

The dominant ionization process at low latitudes is photoionization (Moore et al., 2006, 2010, 2018; Schunk & Nagy, 2009). This can be represented by

$$\begin{aligned} h\nu + H_2 &\rightarrow H_2^+ + e \quad (\approx 90\%) \\ &\quad H^+ + H + e \quad (\approx 10\%) \end{aligned} \tag{1}$$

The H_2^+ production rate, P_{H2+}, can be obtained via standard aeronomical techniques (cf. Schunk & Nagy, 2009) using a solar radiation spectrum and photoionization cross sections versus wavelength. The solar flux at different altitudes must include optical depth effects that depend on wavelength and solar zenith angle. The peak ion production rate takes place where the optical depth equals unity level for a typical extreme ultraviolet photon (e.g., ≈50 nm). For solar zenith angles appropriate for the proximal orbits ($\chi \approx 20°$) and for H_2 gas, this level corresponds to a vertical column density of $N_{H2} \approx 10^{17}$ cm^{-3} or density of $n_{H2} \approx N/H_n \approx 10^{10}$ cm^{-3}, which is found near CA. At high altitudes, the ionization frequency, or ion production rate per neutral molecule, depends only on the solar flux and cross sections and is equal to $I_{H2+0} = 1.2 \times 10^{-9}$ s^{-1} (Galand et al., 2009; Moore et al., 2010), including a ≈10% photoelectron contribution. Theoretical peak H_2^+ production rates are ≈10 cm^{-3}/s at Saturn (cf. Moore et al., 2018). H^+ ions are mainly produced by dissociative photoionization of H_2 with ionization frequency $I_{H+0} \approx 0.1\ I_{H2+0}$.

Ion-neutral chemistry changes the ion composition and ultimately produces a set of "terminal" ion species, which rapidly undergo electron-ion recombination. Figure 3 displays a simple chemical scheme. Species M and R are explained later. Empirical photochemical equilibrium (PCE) ion densities are calculated in this paper. The key PCE assumption is that local production equals local for each species, s, (i.e., $P_s = L_s$). See Schunk and Nagy (2009).

The main chemical loss of H_2^+ ions, and source of H_3^+ ions, is reaction of H_2^+ with H_2:

$$H_2^+ + H_2 -> H_3^+ + H \quad k_2 = 2 \times 10^{-9} \mathrm{cm}^3 \mathrm{s}^{-1}. \tag{2}$$

All individual rate coefficients used in this paper can be found in Anicich (2003). PCE requires that $I_{H2+}(r)\ n_{H2} = k_2\ n_{H2+}$. The H_2^+ density can be written as $n_{H2+} = P_{H2+}/(k_2\ n_{H2})$, and we also find that $I_{H2+}(r) = P_{H2+}/n_{H2}$, where we have subsumed optical depth effects into $I_{H2+}(r)$. Radial distance is denoted by r. See Figure 2. Note that at higher altitudes, $I_{H2+}(r) = I_{H2+0} \approx 10^{-9}$ s^{-1}, independent of location. The decrease in $I_{H2+}(r)$ near CA is consistent with an EUV optical depth of $\tau \approx 0.7$. The sharp falloff of ionization frequency near latitude $\lambda \approx -15°$ (also seen in the H_2^+ density in Figure 1) is due to the shadow of the optically thick B ring (Hadid et al., 2018).

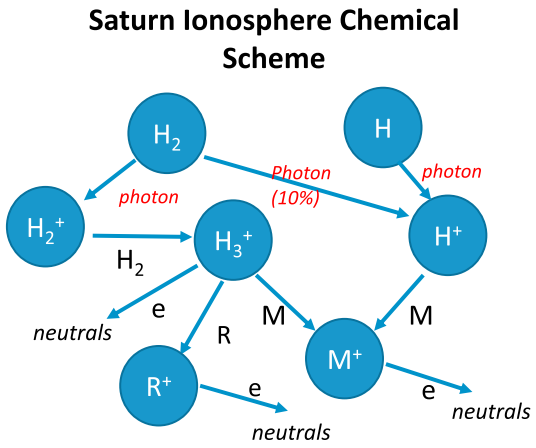

Figure 3. Schematic of the ion chemistry. Photoionization of neutral H_2 and H initiates a series of reactions ending up in dissociative recombination reactions of the generic heavy ion species M^+ and R^+. The chemical role of postulated heavy molecular species M (e.g., CH_4 and H_2O) and R is illustrated. Species R is assumed to only react with H_3^+ and could include N_2. PCE = photochemical equilibrium; RPWS = Radio and Plasma Wave Science.

H_3^+ ions produced by reaction (2) can be chemically removed by dissociative recombination with rate coefficient of $\alpha_1 = 2 \times 10^{-7}$ cm^3/s (Larsson et al., 2008) at electron temperature $T_e \approx 1{,}000$ K (RPWS measurements—Wahlund et al., 2017).

$$H_3^+ + \ e -> H_2 + H \ \ \alpha_3 = 2 \times 10^{-7} cm^3 s^{-1}. \quad (3)$$

The H_3^+ density can be estimated by dividing the empirical H_2^+ production rate from equation (1) by the loss rate from reaction (3) to give $n_{H3+} \approx 5{,}000$ cm^{-3} near CA. This value is much greater than the measured density of ≈100 cm^{-3} (see Figure 1) indicating that an additional H_3^+ loss is needed. The next section introduces heavier neutral and ion molecular species as needed to explain measured H^+, H_3^+, and electron densities.

5. Heavy Molecular Ions and the Electron Density

INMS measured heavier neutral species including H_2O, CH_4, CO_2, and organic compounds in the upper atmosphere (denoted M and R in Figure 3; W18). In this section, we describe how such neutrals react with both H^+ and H_3^+ and produce heavier molecular ion species not detectable by INMS (M^+ and R^+ in Figure 3). The heavy ion species explain the gap evident in Figure 1 between the total light ion density and the electron density. We postulate a set of neutral molecular species, M, with generic total density n_M, or generic mixing ratio (by volume) of $f_M = n_M/n_{H2}$. Reaction of M with H^+ and/or H_3^+ produces a set of heavy ion species, denoted M^+. The resulting M^+ species could include H_2O^+, H_3O^+, CO_2^+, and CH_3^+. For example, the reaction for methane is $H^+ + CH_4 \rightarrow CH_3^+ + H + H$ (rate coefficient $k_{H+CH4} = 4.5 \times 10^{-9}$ cm^3/s). We represent all this chemistry with the generic reaction:

$$H^+ + \ M \rightarrow M^+ \ + \text{neutrals}. \quad (4)$$

An effective (or species-averaged) rate coefficient for H^+ can be defined:

$$k_{Meff} f_M \approx \sum_j k_j f_j \ \text{ and } \ f_M = \sum_j f_j. \quad (5)$$

The summations are over all neutral molecular species, *j*, that react with H^+ (each with mixing ratio, f_j). We adopt relative percentages of various species from the INMS neutral data (W18): CH_4 (35%), CO_2 (10%), H_2O (30%), NH_3 (20%), and also C_2H_4 (5%), excluding mass 28 species (as discussed below). The effective H^+ rate coefficient (i.e., the rate coefficient averaged over different heavy species) is $k_{Meff} = 5.0 \times 10^{-9}$ cm^3/s, differing only by 10% from a rate coefficient for pure methane. Generally, H_3^+ ions react with the same molecular species as H^+, but with somewhat different rate coefficients, k_j. For example, the reaction with methane is $H_3^+ + CH_4 \rightarrow CH_5^+ + H_2$ ($k_{H3+M} \approx 2.4 \times 10^{-9}$ cm^3/s). The effective rate coefficient for H_3^+ loss by species M is $k_{H3+Meff} \approx 3.5 \times 10^{-9}$ cm^3/s.

H_3^+ densities are less than H^+ densities at low altitudes (or low latitude; see Figure 1), suggesting that that H_3^+ also reacts with additional neutral species that do not react with H^+. For example, N_2 and CO could fulfill this role—see Moore et al. (2018). We denote this new generic neutral species R (see Figure 3). We adopt rate coefficients for dissociative recombination of M^+ and R^+ species that are typical (i.e., the CH_3^+ rate coefficient): $\alpha_3 \approx 7 \times 10^{-7}$ $(300/T_e)^{0.61}$ $cm^3/s \approx 3.3 \times 10^{-7}$ cm^3/s (Richard et al., 2012). M^+ and R^+ are the heavier molecular ion species resulting from the chemistry (Figure 3).

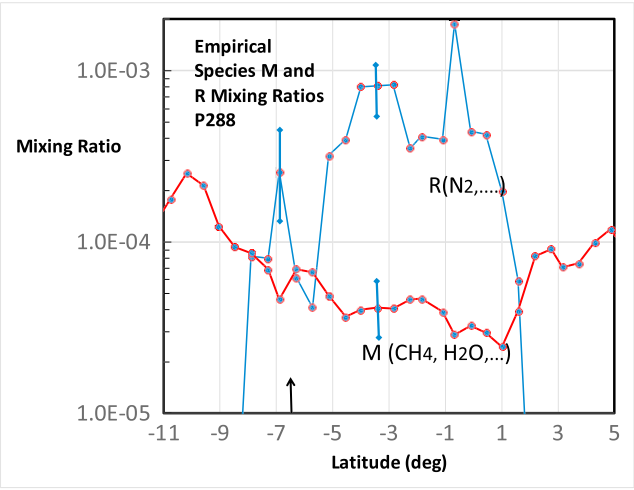

Figure 4. Empirically derived mixing ratios versus latitude for the heavy composite molecular species M and R and for proximal orbit P288. As discussed in the text, species M is assumed to react with both H^+ and H_3^+, and species R only to react with H_3^+. Estimated uncertainities are shown. Closest approach is noted by the upward arrow at the bottom.

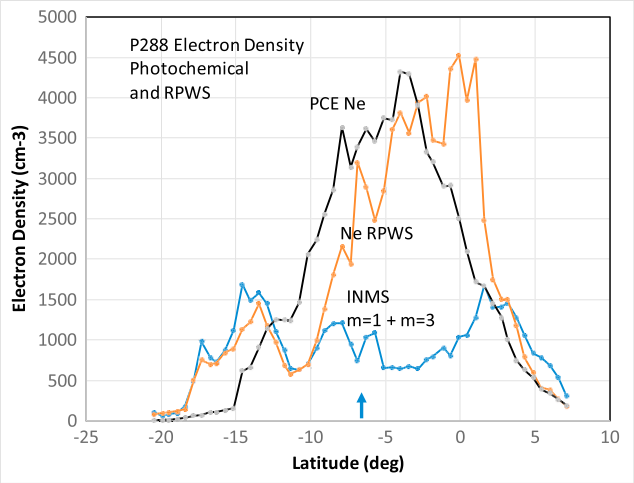

Figure 5. Electron density measured by Radio and Plasma Wave Science (RPWS) versus latitude (orange line), a photochemically determined electron density denoted photochemical equilibrium (PCE; i.e., found using Figure 3 ionization rates and INMS-measured neutral densities—gray line). The total light ion density measured by INMS is also shown. Closest approach is noted by the upward arrow at the bottom.

The densities of the light ion species and the electron densities are taken from Cassini data (Figure 1), and we use a two-step photochemical analysis to deduce mixing ratios for species M and R, f_M, and f_R, respectively. The H^+ PCE expression is rearranged to give $f_M = 0.1\ l_{H2+}/(k_M\ n_{H+})$. l_{H2+} was already discussed and measurements are used for n_{H+}. The dissociative ionization fraction is 0.1. The neutral species M mixing ratios obtained are shown in Figure 4. Note that $f_M \approx 0.5 \times 10^{-4}$ (or 50 ppmv) near the equator and/or at low altitudes, but f_M is larger at higher altitudes, which implies that species M (e.g., CH_4) has an external source (such as the rings; see other special issue papers).

Now, we use H_3^+photochemistry to find the mixing ratio of neutral species R (i.e., the non-H^+ reacting neutral):

$$f_R + f_M \approx [l_{H2+}/n_{H3+} - \alpha_3(N_e/n_{H2})]/k_R. \quad (6)$$

where $k_R \approx k_{H3+Meff}$ is adopted. RPWS Langmuir Probe data are used for N_e and INMS data used for n_{H2} and n_{H3+} (all shown in Figure 1). The resulting empirical mixing ratios, f_R, are shown in Figure 4. Estimated uncertainties in the derived mixing ratios are shown and become large far from CA. It is evident that f_R decreases with latitude away from the equator and/or CA, unlike f_M, which increases. The different altitude/latitude variations of the mixing ratios for M and R suggest that they have different sources.

The major ion species appears to be a collection of heavier molecular ion species with density $n^+_{heavy} = n_{M+} + n_{R+}$. The total ion density (heavy plus light species) must equal the electron density, N_e, plus the densities of any negative ion species or grains (see Morooka et al., 2019) in order to enforce quasi-neutrality. The role of grains and negative ions needs to be further explored (e.g., Morooka et al., 2019), but for now we assume that $n^+_{heavy} \approx N_e$. Balancing source and sink of all ions (and electrons), we get $l_{H2+}\ n_{H2} \approx \alpha_{M/R}\ N_e^2$. Solving this balance equation (cf. Schunk & Nagy, 2009) gives this rough estimate:

$$N_e \approx \left(l_{H2+}/\alpha_{M/R}\right)^{1/2}(n_{H2})^{1/2}. \quad (7)$$

Using l_{H2+} from the present paper (Figure 2) and n_{H2} from INMS data, the derived electron densities are shown in Figure 5 and are compared with measured N_e. The model electron density has a maximum where the H_2^+ production rate has a maximum, roughly at CA, as does the measured N_e (also see Moore et al., 2018).

6. Discussion

This paper demonstrated the existence of one or more heavy molecular ion species in the equatorial ionosphere that can explain the density gap in Figure 1. The analysis indicated that a neutral molecular (M) species exists that reacts with H^+ and H_3^+. The empirically deduced mixing ratio is $f_M \approx 10^{-4}$ and f_M increases with altitude suggesting a high-altitude (i.e., ring) source. The high-mass species mixing ratios from INMS neutral data are similar (W18; Perry et al., 2018). Note that the methods are mostly independent. The surprisingly high mixing ratios are associated with high downward diffusive fluxes of 10^8–10^9 cm^{-2}/s of heavy neutrals such as CH_4 (Koskinen & Guerlet, 2018; Perry et al., 2018; Yelle et al., 2018). Note that the measurements, neutral and ion, were made well above the homopause and cannot be explained by upward diffusion (see Koskinen et al., 2015).

The other heavy neutral species, R, deduced from the ion chemistry has a mixing ratio that decreases with increasing altitude, suggesting a different source for R than for M and not entirely external. But given that altitude and latitude are at least partially confounded variables for the proximal orbits, one could also state that species R is more highly confined to the equatorial region than M. Perhaps the source of R is heavy neutrals generated by ablation of grains entering the atmosphere from the rings (Hamil et al., 2018; Mitchell et al., 2018; Moses & Bass, 2000; Moses & Poppe, 2017).

7. Summary

Cassini INMS ion composition measurements of Saturn's equatorial ionosphere, plus measurements by other Cassini instruments, tell us the following about the ionosphere and its ring interaction:

1. The light ion species (H^+, H_2^+, H_3^+, and He^+) observed by INMS were those expected theoretically prior to the Cassini proximal orbits, but quantitatively the H^+ and H_3^+ densities were lower than predicted.
2. Quantitatively, explaining the measured H^+ and H_3^+ requires surprisingly high abundances of heavy neutral molecular species (e.g., water, methane, and organic compounds) in the ionosphere, with an overall mixing ratio of ≈100 ppmv. Cassini data suggest that these species are due to inputs from the rings, either as gas or as grains.

Acknowledgments
The research described in this paper has been supported by NASA Prime contract NAS7-03001 under JPL subcontract 1405853 to the Southwest Research Institute and SWRI subcontract to the University of Kansas. The research at the University of Iowa was supported by NASA through contract 1415150 with the Jet Propulsion Laboratory. Please see the supporting information for data used in creating the figures.

References

Anicich, V. G. (2003). An index of the literature for bimolecular gas phase cation-molecule. Reaction kinetics. JPL Publication 03–19. Trs-new. jpl.nasa.gov/dspace/bitstream/2014/7981/1/03-2964.pdf

Connerney, J., & Waite, J. H. (1984). New model of Saturn's ionosphere with an influx of water from the rings. *Nature*, *312*(5990), 136–138. https://doi.org/10.1038/312136a0

Galand, M., Moore, L., Charnay, B., Mueller-Wodarg, I., & Mendillo, M. (2009). Solar primary and secondary ionization at Saturn. *Journal of Geophysical Research*, *114*, A06313. https://doi.org/10.1029/2008JA013981

Hadid, L. Z., Morooka, W., Wahlund, J.-E., Moore, L., Cravens, T. E., Hedman, M. M., et al. (2018). Ring shadowing effects on Saturn's ionosphere: Implications for ring opacity and plasma transport. *Geophysical Research Letters*, *45*, 10,084–10,092. https://doi.org/10.1029/2018GL079150

Hamil, O., Cravens, T. E., Reedy, N., & Sakai, S. (2018). Fate of ice grains in Saturn's ionosphere. *Journal of Geophysical Research: Space Physics*, *123*, 1429–1440. https://doi.org/10.1002/2017JA024616

Kaiser, H. L., Desch, M. D., & Connerney, J. E. P. (1984). Saturn's ionosphere: Inferred electron densities. *Journal of Geophysical Research*, *89*(A4), 2371–2376. https://doi.org/10.1029/JA089iA04p02371

Kliore, A. J., Nagy, A. F., Marouf, E. A., Anabtawi, A., Barbinis, E., Fleischman, D. U., & Kahan, D. S. (2009). Midlatitude and high-latitude electron density profiles in the ionosphere of Saturn obtained by Cassini radio occultation observations. *Journal of Geophysical Research*, *114*, A04315. https://doi.org/10.1029/2008JA013900

Kliore, A. J., Patel, I. R., Lindal, G. F., Sweetnam, D. N., & Hotz, H. B. (1980). Structure of the ionosphere and atmosphere of Saturn from Pioneer 11 Saturn radio occultation. *Journal of Geophysical Research*, *85*(A11), 5857–5870. https://doi.org/10.1029/JA085iA11p05857

Koskinen, T. T., & Guerlet, S. (2018). Atmospheric structure and helium abundance on Saturn from Cassini/UVIS and CIRS observations. *Icarus*, *307*, 161–171. https://doi.org/10.1016/j.icarus.2018.02.020

Koskinen, T. T., Sandel, B. R., Yelle, R. V., Strobel, D. F., Mueller-Wodarg, I. C. F., & Erwin, J. T. (2015). Saturn's variable thermosphere from Cassini/UVIS occultations. *Icarus*, *260*, 174–189. https://doi.org/10.1016/j.icarus.2015.07.008

Larsson, M., Mccally, B. J., & Orel, A. E. (2008). The dissociative recombination of H_3^+—A saga coming to the end. *Chemical Physics Letters*, *462*(4-6), 145–151. https://doi.org/10.1016/j.cplett.2008.06.069

Mitchell, D. G., Perry, M. E., Hamilton, D. C., Westlake, J., Kollmann, P., Smith, H. T., et al. (2018). Dust grains fall from Saturn's D-ring into its equatorial upper atmosphere. *Science*, *362*. https://doi.org/10.1126/science.aat2236

Moore, L., Cravens, T. E., Müller-Wodarg, I., Perry, M. E., Waite, J. H. Jr., Perryman, R., et al. (2018). Models of Saturn's equatorial ionosphere based on in situ data from Cassini's Grand Finale. *Geophysical Research Letters*, *45*, 9398–9407. https://doi.org/10.1029/2018GL078162

Moore, L., Mueller-Wodarg, I., Galand, M., Kliore, A., & Mendillo, M. (2010). Latitudinal variations in Saturn's ionosphere: Cassini measurements and model comparisons. *Journal of Geophysical Research*, *115*, A11317. https://doi.org/10.1029/2010JA015692

Moore, L., Nagy, A. F., Kliore, A. J., Müller-Wodarg, I., Richardson, J. D., & Mendillo, M. (2006). Cassini radio occultations of Saturn's ionosphere: Model comparisons using a constant water flux. *Geophysical Research Letters*, *33*, L22202. https://doi.org/10.1029/2006GL027375

Morooka, M. W., Wahlund, J.-E., Hadid, L. Z., Eriksson, A. I., Edberg, N. J. T., Vigren, E., et al. (2019). Saturn's dusty ionosphere. *Journal of Geophysical Research: Space Physics*, *124*, 1679–1697. https://doi.org/10.1029/2018JA026154

Moses, J., & Bass, S. (2000). The effects of external material on the chemistry and structure of Saturn's ionosphere. *Journal of Geophysical Research*, *105*(E3), 7013–7052. https://doi.org/10.1029/1999JE001172

Moses, J. I., & Poppe, A. R. (2017). Dust ablation on the giant planets: Consequences for stratospheric photochemistry. *Icarus*, *27*, 33–58.

Mueller-Wodarg, I., Mendillo, M., Yelle, R., & Aylward, A. (2006). A global circulation model of Saturn's thermosphere. *Icarus*, *180*(1), 147–160. https://doi.org/10.1016/j.icarus.2005.09.002

Nagy, A. F., Kliore, A. J., Marouf, E., French, R., Flasar, M., Rappaport, N. J., et al. (2006). First results from the ionospheric radio occultations of Saturn by the Cassini spacecraft. *Journal of Geophysical Research*, *111*, A06310. https://doi.org/10.1029/2005JA011519

O'Donoghue, J., Stallard, T. E., Melin, H., Jones, G. H., Cowley, S. W. H., Miller, S., et al. (2013). The domination of Saturn's low-latitude ionosphere by ring "rain". *Nature*, *496*(7444), 193–195. https://doi.org/10.1038/nature12049

Perry, M. E., Waite, J. H. Jr., Mitchell, D. G., Miller, K. E., Cravens, T. E., Perryman, R. S., et al. (2018). Material flux from the rings of Saturn into its atmosphere. *Geophysical Research Letters*, *45*, 10,093–10,100. https://doi.org/10.1029/2018GL078575

Persoon, A. M., Kurth, W. S., Gurnett, D. A., Groene, J. B., Sulaiman, A. H., Wahlund, J.-E., et al. (2019). Electron density distributions in Saturn's ionosphere. *Geophysical Research Letters*, *45* 3061–3068. https://doi.org/10.1029/2018GL078020

Richard, T., Kashperka, I., Vigren, E., & Geppert, W. D. (2012). Dissociative recombination of vibrationally excited cold CH3+ and interstellar implications. *American Astronomical Society*, *758*(1), 55. https://doi.org/10.1088/0004-637x/758/1/55

Schunk, R. W., & Nagy, A. F. (2009). *Ionospheres: Physics, plasma physics, and chemistry* (2nd ed.). Cambridge, UK: Cambridge University Press. https://doi.org/10.1017/CBO9780511635342

Teolis, B., Perry, M., Magee, B., Westlake, J., & Waite, J. H. (2010). Detection and measurement of ice grains and gas distribution in the Enceladus plume by Cassini's Ion Neutral Mass Spectrometer. *Journal of Geophysical Research*, *115*, A09222. https://doi.org/10.1029/2009JA015192

Wahlund, J.-E., Morooka, M. W., Hadid, L. Z., Persoon, A. M., Farrell, W. M., Gurnett, D. A., et al. (2017). In situ measurements of Saturn's ionosphere show that it is dynamic and interacts with the rings. *Science*, *359*(6371), 66–68. https://doi.org/10.1126/science.aao4134

Waite, J. H., Atreya, S. K., & Nagy, A. F. (1979). The ionosphere of Saturn: Predictions for Pioneer 11. *Geophysical Research Letters*, *6*(9), 723–726. https://doi.org/10.1029/GL006i009p00723

Waite, J. H. Jr., Lewis, W. S., Kasprzak, W. T., Anicich, V. G., Block, B. P., Cravens, T. E., & Yelle, R. V. (2004). The Cassini ion and neutral mass spectrometer (INMS) investigation. *Space Science Reviews*, *114*(1-4), 113–231. https://doi.org/10.1007/s11214-004-1408-2

Waite, J. H., Perryman, R. S., Perry, M. E., Miller, K. E., Bell, J. M., Cravens, T. E., et al. (2018). INMS observations of chemical interactions between Saturn's atmosphere and rings. *Science*, *362*. https://doi.org/10.1126/science.aat2382

Yelle, R. V., Serigano, J., Koskinen, T. T., Hörst, S. M., Perry, M. E., Perryman, R. S., & Waite, J. H. Jr. (2018). Thermal structure and composition of Saturn's upper atmosphere from Cassini/Ion Neutral Mass Spectrometer measurements. *Geophysical Research Letters*, *45*, 10,951–10,958. https://doi.org/10.1029/2018GL078454